AUTHOR CORRECTION

Rappoport, J. Z. and Simon, S. M. (2003). Real-time analysis of clathrin-mediated endocytosis during cell migration. *J. Cell Sci.* **116**, 847-855.

In both the online and print versions of this paper, in Materials and Methods, the construct pEGFP-dynamin2 was incorrectly identified as a human isoform. It is a rat isoform.

Real-time analysis of clathrin-mediated endocytosis during cell migration

Joshua Z. Rappoport and Sanford M. Simon*

The Laboratory of Cellular Biophysics, The Rockefeller University, 1230 York Avenue, Box 304, New York, NY 10021, USA
*Author for correspondence (e-mail: simon@rockefeller.edu)

Summary

Simultaneous dual-color total-internal-reflection fluorescence microscopy (TIR-FM) was performed to analyze the internalization and distribution of markers for clathrin-mediated endocytosis (clathrin, dynamin1, dynamin2 and transferrin) in migrating cells. In MDCK cells, which endogenously express dynamin2, the dynamin2-EGFP fluorescence demonstrated identical spatial and temporal behavior as clathrin both prior to and during internalization. By contrast, in the same cells, the neuronal dynamin1 only localized with clathrin just prior to endocytosis. In migrating cells, each endocytic marker was polarized towards the leading edge, away from the lagging edge. These observations suggest a re-evaluation of the functional differences between dynamin1 and dynamin2, and of the role of clathrin-mediated endocytosis in cell migration.

Movies available online

Key words: Endocytosis, Clathrin, Dynamin, Cell migration, Total internal reflection fluorescence microscopy (TIR-FM), Evanescent-wave microscopy

Introduction

The internalization of integral membrane proteins from the cell surface through receptor-mediated endocytosis occurs via clathrin-coated pits (Schmid, 1997; Takei and Haucke, 2001). Examples of molecules that undergo clathrin-mediated endocytosis include nutrients such as iron, via transferrin uptake (Hopkins et al., 1985; Conrad et al., 1999), growth factors and cytokines, through receptors such as the epidermal-growth-factor receptor (Lamaze and Schmid, 1995; Carter and Sorkin, 1998), and cellular adhesion molecules such as integrins (Raub and Kuentzel, 1989). Additionally, numerous pathogenic organisms and molecules have been observed to gain entry into cells by exploiting the endocytosis machinery (Doxsey et al., 1987; Sieczkarski and Whittaker, 2002). Endocytosis has also been implicated in cell migration (Bretscher, 1996; Palecek et al., 1996; Sheetz et al., 1999; Bajno et al., 2000; Kamiguchi and Lemmon, 2000). In particular, it has been proposed that an increased rate of endocytosis at the trailing edge would contribute to the polarized cycling of either bulk membrane or cellular adhesion molecules, such as integrins, to the leading edge (Bretscher, 1996; Palecek et al., 1996; Sheetz et al., 1999).

Great strides have recently been made in the analysis of the different factors involved in the production of clathrin-coated vesicles (Takei and Haucke, 2001). The presence and interaction of such components as the AP-2 adapter complex (Benmerah et al., 1998; Kamiguchi et al., 1998) and the accessory proteins AP180 (Takei and Haucke, 2001), Eps15 (Benmerah et al., 1998; Benmerah et al., 1999) and Hip1R (Engqvist-Goldstein et al., 2001) are beginning to be well characterized. Many of the proteins that are involved in clathrin-mediated endocytosis have been identified and cloned, their crystal structures have been determined (ter Haar et al., 1998; Collins et al., 2002), and detailed models for the production and internalization of clathrin-coated vesicles have been suggested (Schmid, 1997; Takei and Haucke, 2001; Kirchhausen, 2002). However, numerous questions regarding the events and interactions relevant to endocytosis remain unanswered. For example, it is not clear whether activated receptors recruit AP-2 which results in the polymerization of clathrin coat components, or if clathrin-coated pits are preformed and recruit activated receptors. Additionally, the precise molecular function(s) of the GTPase dynamin in endocytosis remains to be resolved (Takei et al., 1995; Cao et al., 1998; McNiven et al., 2000; Ochoa et al., 2000; Schmid and Sorkin, 2002; Tsuboi et al., 2002). Although previous studies have focused on the neuron-specific dynamin1 isoform (Tsuboi et al., 2002), there is also a functional role in endocytosis for the ubiquitously expressed dynamin2. Dynamin2-enhanced green fluorescent protein (EGFP) colocalizes with endogenous clathrin (Cao et al., 1998). Dominant negative mutants of dynamin1 and dynamin2 both reduce endocytosis (Altschuler et al., 1998; Sun et al., 2002) and non-functional dynamin forms rings that wrap around the neck of latent vesicles (Takei et al., 1995). These observations have led to the hypothesis that dynamin associates with the neck of the budding vesicle to play a key role in membrane fission.

The present studies have made use of simultaneous dual-color total-internal-reflection fluorescence microscopy (TIR-FM) to characterize the dynamics and interactions of components of the endocytosis machinery. In TIR-FM, the fluorescence excitation is limited to a depth of ~100 nm from the cover slip. This both minimizes photodamage to the cell

and maximizes the signal over background of fluorophores at the cell surface (Axelrod, 1981; Schmoranzer et al., 2000; Lampson et al., 2001). Previously, our laboratory has employed TIR-FM in the study of constitutive exocytosis (Schmoranzer et al., 2000) and in an investigation of the endosomal recycling compartment (Lampson et al., 2001). Using this approach to examine both the distribution of the components of the endocytic machinery and the distribution of endocytic sites allowed us to examine whether endocytosis is polarized or occurs uniformly in migrating cells. Clathrin was expressed as plasma-membrane-associated spots, which displayed apparently stochastic internalization. Whereas dynamin2, which is endogenously expressed in these cells, colocalized with clathrin both prior to and during internalization, the neuronal dynamin1 only appeared just prior to the disappearance of the clathrin spots. Finally, contrary to our expectations, clathrin-mediated endocytosis was polarized away from the lagging edge of migrating cells, being concentrated towards the leading edge.

Materials and Methods

Plasmid constructs

The construct encoding dsRed-clathrin (rat light chain) was a gift from Thomas Kirchhausen (Harvard Medical School, Boston, MA). pEGFP-dynamin2 (human isoform aa) was a gift from Mark McNiven (The Mayo Clinic, Rochester, MI). pEGFP-dynamin1 (human isoform aa) was a gift from Pietro de Camilli (Yale University, New Haven, CT). pECFP-Mem was purchased from Clontech (BD Biosciences Clontech, Palo Alto, CA).

Cell culture and monolayer wounding assay

Madine Darby Canine Kidney (MDCK) cells were maintained in DMEM (Mediatech Cellgro, VA) supplemented with 10% fetal bovine serum in a humidified 37°C incubator with 5% CO_2. Cells were plated onto sterilized glass cover slips (Fisher Scientific, Atlanta, GA). When cells were transfected with dsRed-clathrin, cells were plated at approximately confluence and transfected during plating utilizing Lipofectamine 2000 (Invitrogen, Carlsbad, CA) according to the supplier's directions. Cells co-transfected with dsRed-clathrin and ECFP-Mem, or dsRed-clathrin and dynamin1-EGFP, were plated between 75% and 95% confluence the day prior to transfection. In each case where migrating cells were analyzed, when cells had reached or nearly reached confluence, the monolayer was wounded with a scalpel; a circular region ~1 cm in diameter was removed from the center of the monolayer. The morning after wounding, some cells were microinjected with pEGFP-dynamin2 at 50 ng μl^{-1} using continuous flow through the microinjection pipette. Cells within the migrating front were imaged between 6 hours and 43 hours after wounding.

Cell surface transferrin staining

Approximately 16 hours after wounding, cells were placed in serum-free DMEM for 30 minutes in a 37°C incubator to chase out any cell-surface-bound transferrin. Cells were then placed in Alexafluor488-transferrin (Molecular Probes, Eugene, OR) diluted 1:100 in ice-cold PBS and incubated for 20 minutes at 4°C. Finally, cells were rinsed once in PBS and fixed for 5 minutes in 4% paraformaldehyde (Electron Microscopy Sciences, Fort Washington, PA).

Image acquisition

TIR-FM was performed as previously described (Schmoranzer et al., 2000; Lampson et al., 2001) utilizing illumination through the microscope objective (Apo 60× NA 1.45; Olympus America, Melville, NY). All studies were performed with an inverted epifluorescence microscope (IX-70 Olympus) placed within a home-built temperature controlled enclosure set at 32°C for live cell imaging. The optical configuration used to image dsRed-clathrin included excitation with the 514 nm line of a tunable argon laser (Omnichrome, model 543-AP A01; Melles Griot, Carlsbad, CA) reflected off a polychroic mirror (442/514pc). All filters and polychroic and dichroic mirrors were obtained from Chroma Technologies (Brattleboro, VT). Emitted light was then collected through a 560lp filter.

ECFP-Mem was imaged following excitation by the 442 nm line of a HeCd laser (Omnichrome, model 4056-S-A02), reflected off the same 442/514pc as above. The ECFP emission was collected utilizing a HQ485/40M band pass filter. Dynamin2-EGFP and Alexafuor488-transferrin were excited by the 488 nm line of the argon laser reflected off a dichroic mirror (498DCLP). EGFP and Alexafluor488 emission were collected through an emission band pass filter (HQ525/50M). When dsRed-clathrin and dynamin2-EGFP, or dsRed-clathrin and dynamin1-EGFP, were imaged simultaneously both fluorophores were excited with the 488 nm line of the same tunable argon laser as above reflected off the 498DCLP dichroic. Simultaneous image acquisition was performed utilizing an emission splitter (W-view, Hamamatsu Photonics, Hamamatsu City, Japan). The GFP/dsRed emissions were collected simultaneously through an emission splitter equipped with dichroic mirrors to split the emission (550DCLP). The GFP emission was then collected through an emission band pass filter (HQ525/50M) and the dsRed through an emission long pass filter (580lp). Fluorophore emission cross-talk from the green channel into the red and from the red into the green were both observed to be less than 1% in preliminary control experiments.

The camera utilized to acquire images was a 12-bit cooled CCD (ORCA-ER, Hamamatsu Photonics, Bridgewater, NJ) with a resolution of 1280×1024 pixels (pixel size=6.45 μm × 6.45 μm). The camera and a mechanical shutter (Uniblitz, Vincent Associates, Rochester, NY) were controlled by MetaMorph (Universal Imaging, Downingtown, PA). Images were acquired utilizing exposures times between 150 milliseconds and 300 milliseconds. For video imaging, between 200 and 400 frames were streamed to memory on a PC during acquisition and then saved to hard disk. The depth of the evanescent field was typically ~70-100 nm (Schmoranzer et al., 2000; Lampson et al., 2001). Analysis of video sequences and still frames was done with MetaMorph and Excel (Microsoft, Redmond, WA). For the quantification of dsRed-clathrin spot number and spot internalization a grid of squares (35 pixels × 35 pixels) was placed within each cell region and all of the spots and disappearing spots within the squares were counted. Image noise was reduced through background subtraction and digital brightness and contrast adjustment in MetaMorph and Photoshop (Adobe Systems, San Jose, CA).

Dual-color processing

Dual-color image streams were acquired so that the separated channels appear side by side on the camera chip. Regions of the same size were removed from the whole field to yield separated image sequences. The two channels (GFP and dsRed) were aligned by eye and then correlation coefficients were obtained using automatic thresholding. For both dsRed-clathrin/Alexafluor488-transferrin and dsRed-clathrin/dynamin2-EGFP images, correlation coefficients were obtained following pixel shift of the red image planes, one pixel at a time for ten pixels in each direction. Each of the four resultant correlation coefficients for each pixel shift step was then averaged.

Results

Endocytosis in live cells was studied by following fusions of fluorescent proteins to clathrin (dsRed-clathrin) and dynamin2 (dynamin2-EGFP). The localization and behavior of GFP- or dsRed-clathrin coated pits in living cells has previously been evaluated by epifluorescence imaging (Gaidarov et al., 1999; Engqvist-Goldstein et al., 2001; Santini et al., 2002). In epifluorescence microscopy the clathrin was observed throughout the cell, both in puncta (presumably on the plasma membrane) and in a juxtanuclear region (presumably at the Golgi and on Golgi-derived vesicles). TIR-FM is a useful tool for analyzing events at the basal plasma membrane because it results in a selective excitation of fluorophores within ~100 nm of the cover slip (Axelrod, 1981). Thus, there is a very significant decrease both of out-of-focus fluorescence and of photodamage to the cell (Schmoranzer et al., 2000; Lampson et al., 2001). In TIR-FM, the dsRed-clathrin was found only in discrete puncta in the plasma membrane associated region (Fig. 1A). The juxtanuclear region fluorescence was not excited by TIR-FM. In TIR-FM, the dsRed-clathrin could be imaged at a much faster rate and with a greater signal to noise than with epifluorescence. This was the consequence of a number of factors. First, in TIR-FM, there is substantially reduced background in the absence of out-of-focus light. Second, the higher NA of the TIR-FM objectives meant that much more light was collected. Finally, in these studies, we used cameras with a greater sensitivity, which allowed us to resolve images with a temporal resolution of 1 frame every ~0.3 seconds, compared with 1 frame every 1.4 seconds in previous epifluorescence studies (Engqvist-Goldstein et al., 2001).

In TIR-FM, the clathrin puncta showed similar behaviors to those previously reported (Gaidarov et al., 1999), including lateral movement (Fig. 1B), disappearance (Fig. 1C) and appearance or formation (Fig. 1D; see supplementary Movie 1, http://jcs.biologists.org/supplemental). However, TIR-FM permitted an analysis of the dynamics of clathrin motion and disappearance at a level of sensitivity not previously attained (Santini et al., 2002). Although most of the puncta were relatively static during the time course of each sequence, a subpopulation underwent linear lateral movements parallel to the plane of the membrane (Fig. 1B). The average lateral displacement quantified for sixteen moving spots identified from three cells was 2.16±0.25 μm, and the average lateral speed of these motile spots was 0.84±0.10 μm second^{-1}. This is greater than the speed of actin-based motility for listeria (Goldberg, 2001) or vesicle-based movement (Merrifield et al., 1999) and is consistent with some of the rates of movement of microtubules motors (Apodaca, 2001) and myosin-V-based transport (Tabb et al., 1998).

The fluorescence of some clathrin puncta disappeared. In three cells, a total of 1507 spots were counted and 237 of these disappeared within imaging streams of 60.7±3.5 seconds. The average percentage of spots that disappeared per stream was 14.4±5.4%. The average rate of disappearance calculated for ten spots selected from the cell presented in Fig. 1 was 17.5±4.1 seconds, although some spots disappeared in as little as ~1.2 seconds (Fig. 1E).

To characterize further the dynamics of dsRed-clathrin during endocytosis, its fluorescence was monitored with either a second molecule involved in the machinery of endocytosis (dynamin1 or dynamin2) or a cargo molecule (transferrin). Transferrin has previously been used to study endocytosis in MDCK cells, which are known to express functional transferrin receptor endogenously (Fuller and Simons, 1986; Fialka et al., 1999). Cells were transfected with dsRed-clathrin and the cell surface labeled with Alexafluor488-transferrin in the cold. Numerous transferrin puncta (Fig. 2A) colocalized with dsRed-clathrin (Fig. 2B). The colocalization of transferrin in dsRed-clathrin puncta was quantified by the pixel shift analysis (Fig. 2C). The correlation coefficient between clathrin and transferrin was quantitatively reduced following the deliberate misalignment of the two constituent single channel images.
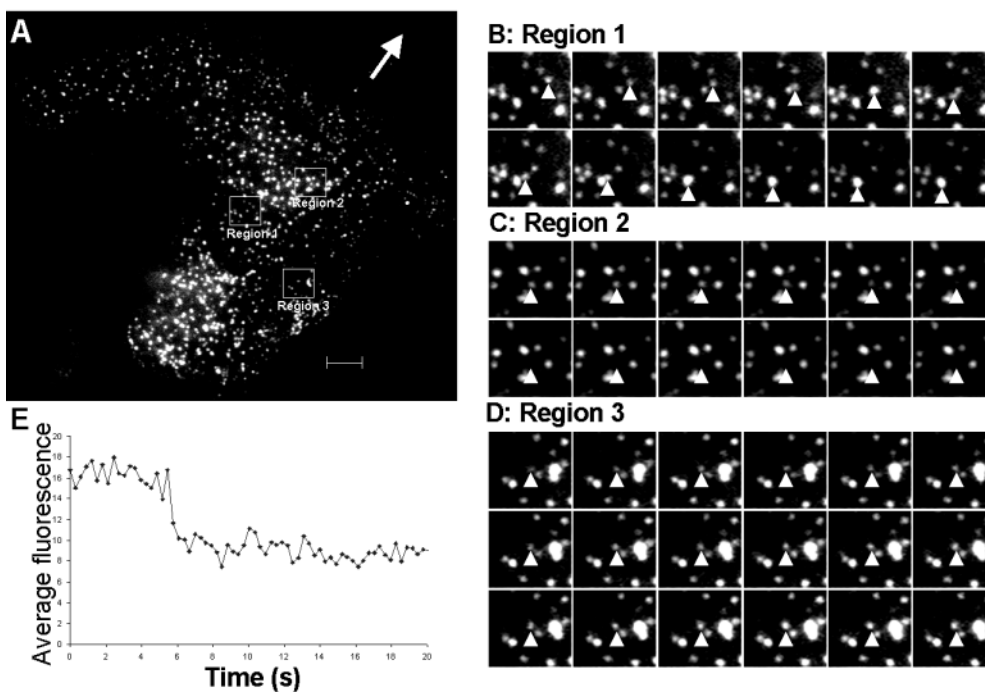
Fig. 1. Analysis of clathrin dynamics in a migrating cell by TIR-FM. (A) A TIR-FM still image (from a sequence taken at 300 milliseconds per frame) demonstrating the presence of numerous dsRed-clathrin basal plasma membrane associated puncta. Scale bar, 5 μm. (B) 12 sequential images taken from an image stream of 200, enlarging region 1 from A. The frames depict the lateral movement of the clathrin punctum marked by the arrowhead. (C) 12 sequential images enlarging region 2 from A. These images depict the disappearance of the clathrin punctum marked by the arrowhead, presumably via internalization. (D) 18 sequential images enlarging region 3 from A, demonstrating the increasing fluorescence at the spot marked by the arrowhead. (E) Quantification of the fluorescence associated with a single disappearing dsRed-clathrin punctum.

Alexa488-Transferrrin   dsRed-clathrin
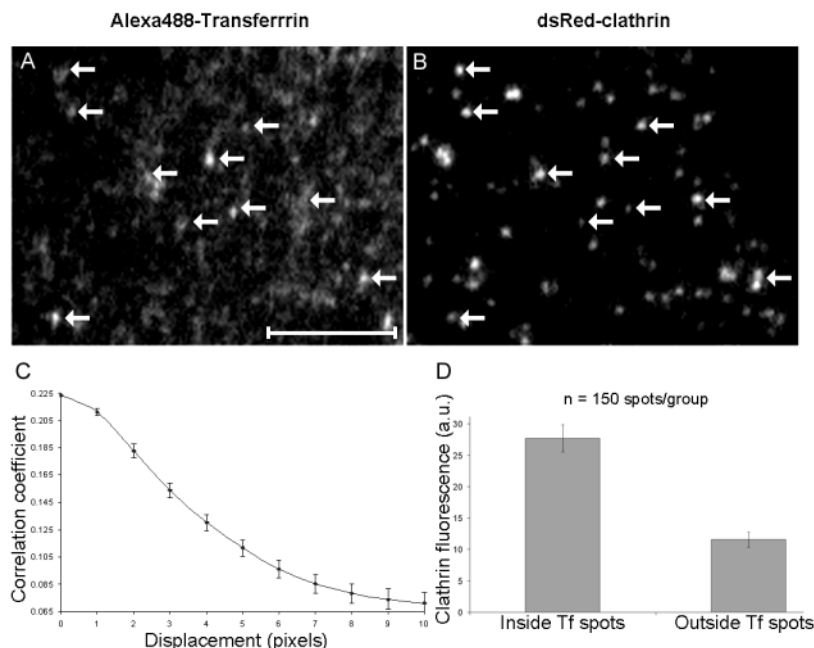
Fig. 2. Colocalization of dsRed-clathrin in Alexafluor488-transferrin puncta. (A) Alexafluor488-transferrin TIR-FM image. (B) dsRed-clathrin TIR-FM image of the same cell as in A. Spots marked by arrows contain both transferrin and clathrin. Scale bar, 5 μm. (C) The decrease of mean ± s.e.m. of correlation coefficient comparing images in A and B following pixel shift in all four directions. (D) Bar graph comparing the average clathrin fluorescence per unit area ± s.e.m. in regions within 150 transferrin puncta (50 per cell) to an equivalent number of regions outside of transferrin spots.

The decrease in correlation coefficient caused by pixel shifting of one channel in the overlay image demonstrates that the colocalization is not due to the random alignment of isolated puncta. Additionally, the clathrin fluorescence associated with a total of 150 transferrin spots (50 per cell) was quantified and compared to the clathrin fluorescence within 150 regions of equal size residing outside of transferrin spots (Fig. 2D). This result confirms the colocalization of clathrin and transferrin at the plasma membrane (Fig. 2D), thus implicating these puncta as functional in the clustering and endocytosis of substrates. A population of clathrin spots did not contain appreciable transferrin (Fig. 2). This suggests that the contents of the cargo within each clathrin-coated pit might not be identical.

Dynamin2 colocalizes with clathrin (Takei et al., 1995) and endocytosis is reduced in cells expressing mutant forms of dynamin2 (Altschuler et al., 1998). To examine the temporal dynamics of the interaction between clathrin and dynamin2, we simultaneously imaged dsRed-clathrin (Fig. 3A,D) and dynamin2-EGFP (Fig. 3B,E). In epifluorescence, there were some regions in which the two proteins colocalized and others where they did not; in the juxtanuclear regions, there was a strong dsRed-clathrin signal without an equivalent quantity of dynamin2 (Fig. 3A-C). However, in TIR-FM, there were only plasma-membrane-based puncta of dsRed-clathrin, each of which colocalized with dynamin2-EGFP (Fig. 3D-F). As observed between clathrin and transferrin (Fig. 2C), the colocalization of clathrin and dynamin2 was reduced following pixel shift analysis (Fig. 3G). Additionally, the dynamin2-
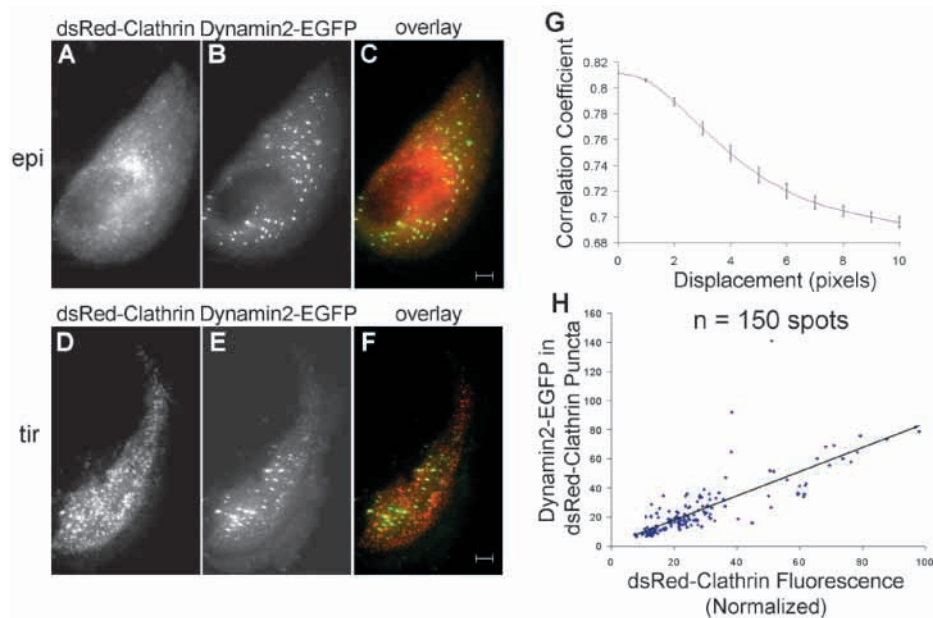
Fig. 3. Colocalization of dynamin2-EGFP in dsRed-clathrin puncta in migrating MDCK cells. (A) dsRed-clathrin epifluorescence image. (B) Dynamin2-EGFP epifluorescence image. (C) Overlay of A and B. Scale bar, 5 μm. (D) dsRed-clathrin TIR-FM image. (E) Dynamin2-EGFP TIR-FM image. (F) Overlay of D and E. Scale bars, 5 μm. (G) Depiction of the decrease of mean ± s.e.m. of correlation coefficient comparing images in D and E following pixel shift in all four directions. (H) Graph of the dynamin2-EGFP fluorescence relative to dsRed-clathrin fluorescence (normalized to whole cell relative fluorophore intensity for each cell) within 150 clathrin puncta from three cells (50 per cell).

EGFP fluorescence present in 150 puncta from a total of three cells was observed to be linearly proportional to the amount of dsRed-clathrin (Fig. 3H).

A number of the dsRed-clathrin/dynamin2-EGFP puncta were observed to disappear stochastically (Fig. 4A-D). In these puncta, the fluorescence of the dsRed-clathrin and the dynamin2-EGFP disappeared synchronously (Fig. 4), and the relative intensity of their fluorescence decreased proportionally in each punctum that disappeared (Fig. 4E). Therefore, it appears that the spatial correlation observed between clathrin and dynamin2 (Fig. 3) persists during the process of endocytosis.

The disappearance of the clathrin/dyanamin2 puncta could be the consequence of photobleaching, lateral movement or endocytosis. It is unlikely to be the consequence of photobleaching because the fluorescence intensity did not decrease in the regions surrounding the spots that disappeared. An example is shown in Fig. 4, where a punctum of clathrin (Fig. 4C) and dynamin (Fig. 4D) disappeared but the fluorescence in the neighboring region did not change. The decrease is unlikely to be the result of lateral motion, because the intensity in the area outside of the spots did not increase over time. Thus, the simultaneous disappearance of the clathrin and dynamin in the punctum is most like the result of an endocytic movement out of the plane of the evanescent field. Because the clathrin and dynamin2 are colocalized and are roughly proportional to each other both before and during endocytosis, there might be a relatively stable stoichiometric relationship between them.

The neuronal dynamin1 is 79% identical to dynamin2. To determine whether the two proteins behave similarly, MDCK cells were co-transfected with dsRed-clathrin and dynamin1-EGFP. As with dynamin2-EGFP, dynamin1-EGFP co-localized with many dsRed clathrin puncta (data not shown). However, in contrast to the behavior of dynamin2-EGFP (Fig. 4E), dynamin1-EGFP fluorescence increased just prior to internalization of dsRed-clathrin spots (Fig. 4F-H). This observation suggests that the behaviors of dynamin1 and dynamin2 prior to and during endocytosis are not identical, although the functional significance of this difference is not yet known.

The use of TIR-FM allows us to quantify the distribution of molecules involved in endocytosis (clathrin and dynamin1/2), endocytic cargo (transferrin) and endocytic events (the simultaneous disappearance of puncta of clathrin and dynamin). It has been proposed that endocytosis occurs at higher rates at the trailing edge of migrating cells. We used our techniques to assay whether there was a polarity of endocytic machinery, cargo or endocytic events in the basal membrane of MDCK cells during movement.

A monolayer of MDCK cells transfected with dsRed-clathrin was wounded with a scalpel. Over a one-hour period, multiple cells expressing various levels of dsRed-clathrin were observed by epifluorescence time-lapse microscopy to migrate towards the area of monolayer wounding (Fig. 5, supplementary Movie 2). Some shape changes were associated with the directed movement of these cells, including the retraction of the lagging edge (see cell on the right hand side
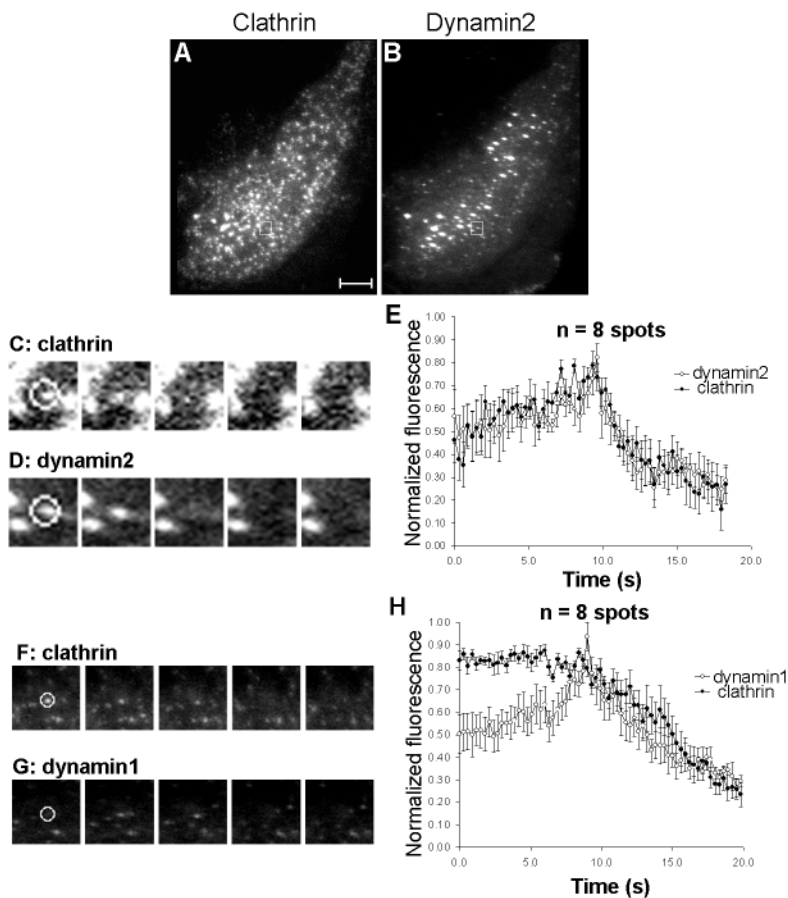
Fig. 4. Colocalization of dynamin2-EGFP and dynamin1-EGFP in disappearing dsRed-clathrin puncta. (A) dsRed-clathrin TIR-FM image. Scale bar, 5 μm. (B) Dynamin2-EGFP TIR-FM image. (C) Five sequential images (300 milliseconds per frame) enlarging area outlined in A. (D) Five sequential images enlarging area outlined in B. (E) Graphic depiction of the disappearance of eight dsRed-clathrin and dynamin2-EGFP containing spots; values are presented as the mean ± s.e.m. of the average fluorescence per unit area relative to maximum value obtained for each spot minus the minimum value for each. (F, G) Five images (300 milliseconds per frame) demonstrating the behavior of dsRed-clathrin (F) and dynamin1-EGFP (G) prior to and during internalization. Images depicted represent frames 0, 50, 100, 150 and 200. (H) Graphic depiction of the disappearance of eight dsRed-clathrin and dynamin1-EGFP containing spots; values are presented as the mean ± s.e.m. of the average fluorescence per unit area relative to maximum value obtained for each spot minus the minimum value for each. Values depicted were taken from an aligned data set of ~40 seconds. In E and H, the fluorescence traces of each of the eight spots evaluated were temporally aligned to the start of dynamin1/2-EGFP fluorescence decrease.

of the field) as well as the extension of leading lamellae. The migration velocity of these cells ranged between 10 µm hour^{-1} and 20 µm hour^{-1}, similar to values derived from previous
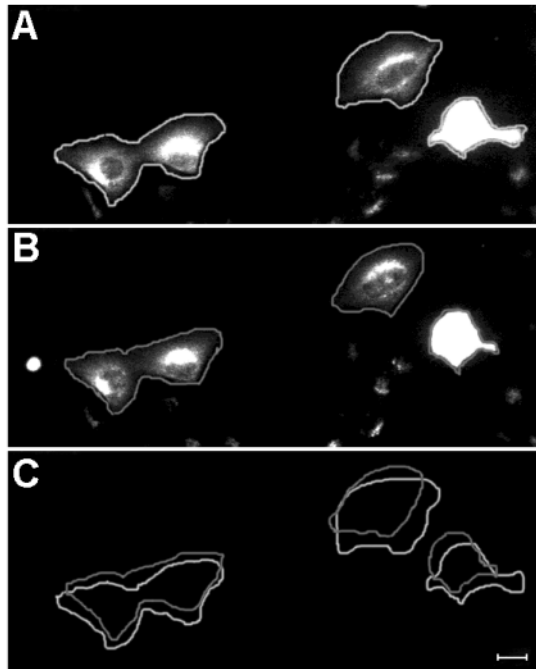
Fig. 5. Migration of MDCK cells transfected with dsRed-clathrin. Cells were imaged via time-lapse epifluorescence microscopy migrating towards the area of monolayer wounding (the top of the field). This figure presents the first (A) and last (B) images of a 1 hour time-lapse sequence, and an overlay (C) of cell borders drawn to illustrate net cell displacement. Scale bar, 20 µm.

studies of MDCK cell migration (Fenteany et al., 2000; Sabo et al., 2001). MDCK cells expressing dynamin2-EGFP were observed to migrate at the same rate in response to monolayer wounding (supplementary Movie 3). These results indicate that MDCK cells migrate normally after monolayer wounding despite the transient expression of dsRed-clathrin or dynamin2-EGFP.

To quantify the distribution of endocytic machinery, cargo and fusion events, we imaged these cells with TIR-FM. At the start of each time-lapse series, an image was collected under epifluorescence, which was used to draw the cell boundaries and demarcate three regions (leading, middle and lagging) along the migratory trajectory of the cell (Fig. 6). Both the dsRed-clathrin signal (Fig. 6B) and the dynamin2-EGFP fluorescence (Fig. 6D) appeared to be weakest at the lagging edge and progressively stronger towards the leading edge of the migrating cells. Quantification of the relative fluorescence per unit area within the three regions of migrating cells revealed similar polarization of clathrin (Fig. 7A), dynamin2 (Fig. 7B) and transferrin (Fig. 7C) fluorescence from lowest values at the lagging edge to highest values at the leading edge. Thus, utilizing TIR-FM to evaluate the distribution of three markers for clathrin-mediated endocytosis revealed that each was concentrated away from the lagging edge.

The observation that the fluorescence of markers for clathrin-mediated endocytosis was lowest at the trailing edge of migrating cells (Figs 6, 7) could be explained if the trailing edge of the cells was not as close to the cover slip as the rest of the cell (the excitatory field decreases exponentially with distance from the cover slip). We tested this possibility by transfecting cells simultaneously with dsRed-clathrin and a marker for the plasma membrane, palmitoylated enhanced cyan fluorescent protein (ECFP-Mem) (Jiang and Hunter,
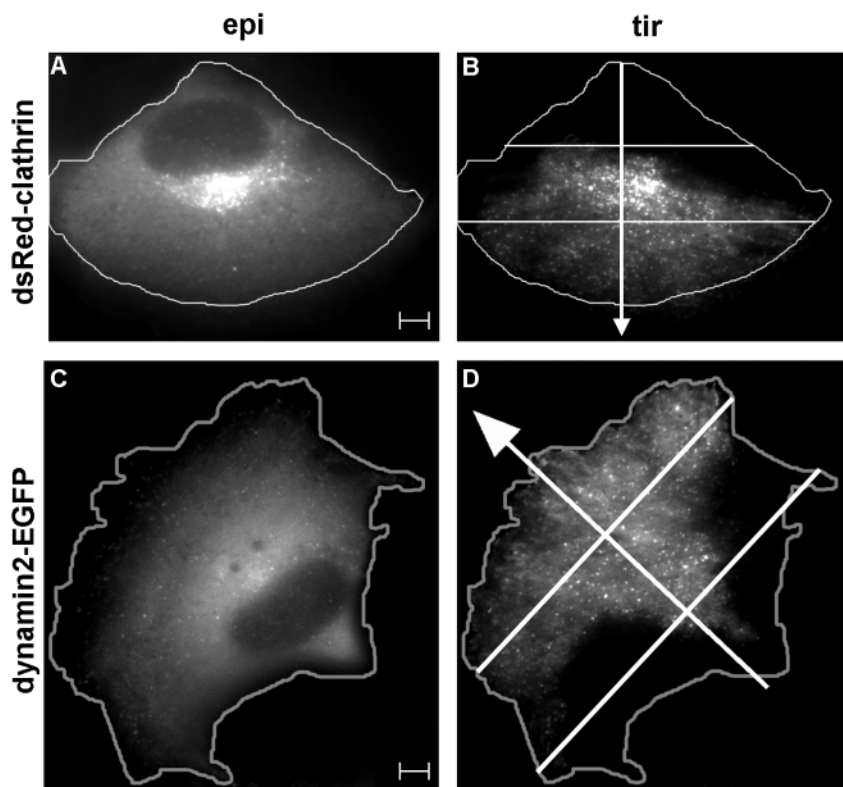
Fig. 6. The distribution of plasma-membrane-associated dsRed-clathrin and dynamin2-EGFP in migrating cells. (A) Epifluorescence image of a migrating MDCK cell expressing dsRed-clathrin. (B) TIR-FM image of the same cell overlying the cell border drawn in A, and depicting the apparent migratory direction of this cell in addition to three regions along this trajectory. (C) Epifluorescence image of a migrating MDCK cell expressing dynamin2-EGFP. (D) TIR-FM image of the same cell overlying the cell border drawn in C, and depicting the apparent migratory direction of this cell in addition to three regions along this trajectory. Scale bar, 5 µm.

1998). The distribution of ECFP-Mem in TIR-FM images should reflect the contact zone between the cell and the cover slip. In cells co-expressing ECFP-Mem (Fig. 8A) and dsRed-clathrin (Fig. 8B) ECFP-Mem was present throughout the basal plasma membrane, whereas dsRed-clathrin was localized to the cell middle and leading edge. Thus, the decreased dsRed signal at the trailing edge is the result of less clathrin in this region and not a greater distance between the plasma membrane and the cover slip. Calculation of the relative dsRed-clathrin

fluorescence per unit area divided by the relative ECFP-Mem intensity per unit area clearly demonstrates that the polarized distribution of dsRed-clathrin fluorescence is not due to variability in distance between the plasma membrane and the cover slip throughout the cell (Fig. 8C). Therefore, the polarized distribution of dsRed-clathrin in the basal membrane is due to differences in protein localization and not to differences in fluorophore excitation.

The preceding results indicate that components of the endocytic machinery (clathrin and dynamin2) and an endocytic cargo (transferrin) are polarized in the plane of the plasma membrane towards the leading edge. To assay endocytic activity, we quantified the density of dsRed-clathrin puncta and frequency with which these puncta disappear. The density of dsRed-clathrin puncta (Fig. 8D) was highest in the leading
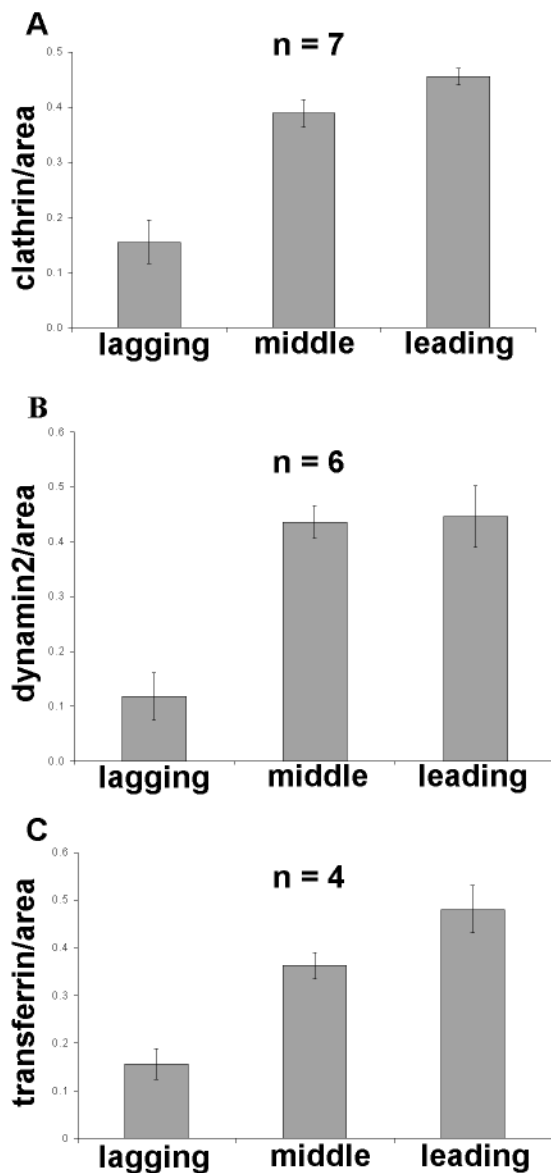
Fig. 7. Polarized distribution of markers for clathrin-mediated endocytosis in the basal membrane of migrating cells. (A) The quantification of the relative dsRed-clathrin fluorescence intensity per unit area within three regions along the migrating axis of the cell. The average of seven cells ± s.e.m. is plotted. (B) The quantification of the relative dynamin2-EGFP fluorescence intensity per unit area within three regions along the migrating axis of the cell. The average of six cells ± s.e.m. is plotted. (C) The quantification of the relative Alexafluor488-transferrin fluorescence intensity per unit area within three regions along the migrating axis of the cell. The average of four cells ± s.e.m. is plotted.
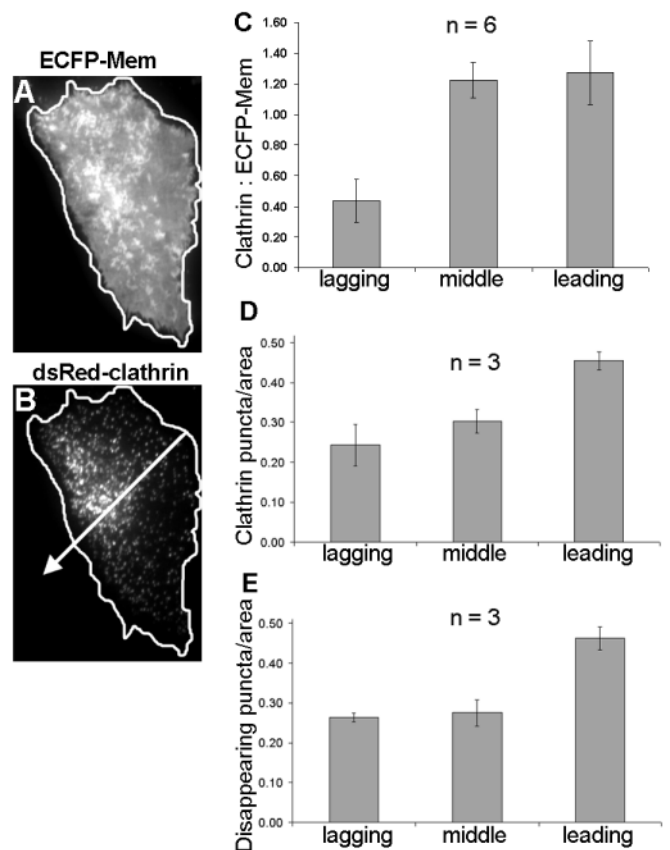
Fig. 8. Distribution of clathrin-mediated endocytosis in the basal plasma membrane of migrating cells. (A) TIR-FM image of the basal plasma membrane ECFP-Mem distribution in a migrating MDCK cell co-transfected with dsRed-clathrin and ECFP-Mem. Cell border was drawn around the entire region of fluorescent signal. (B) dsRed-clathrin TIR-FM image of the same cell overlying the cell border drawn in A. The cell is apparently migrating in the direction denoted by the arrow. (C) The relative dsRed-clathrin fluorescence intensity per unit area divided by the relative ECFP-Mem fluorescence intensity per unit area within three regions of the migrating cell. The average of six cells ± s.e.m. is plotted. (D) The quantification of the relative dsRed-clathrin spot number per unit area within the three cell regions. The average ± s.e.m. is plotted (three cells, 1507 spots). (E) The quantification of the relative dsRed-clathrin spot disappearance per unit area within the three cell regions. The average ± s.e.m. is plotted (three cells, 237 spots).

edge and lowest in the trailing edge, similar to the distribution of the total dsRed-clathrin fluorescence (Fig. 7A, Fig. 8C). Furthermore, the frequency at which the dsRed-clathrin puncta disappeared was enhanced at the leading edge and deceased towards the lagging edge (Fig. 8E). These results suggest that clathrin-mediated endocytosis is polarized towards the leading edge in migrating cells, away from the lagging edge, in contrast to what had been expected.

Discussion

The current observations represent the first simultaneous analysis of clathrin and dynamin in living cells (Figs 3, 4). The ability of TIR-FM selectively to excite fluorophores associated with the plasma membrane has permitted a detailed analysis of the behavior of these markers for endocytosis at a level of sensitivity not previously attained. These results show that, in MDCK cells, clathrin and dynamin2 (the variant that is endogenously expressed in these cells) are colocalized in puncta both during and significantly before internalization (Figs 3, 4). By contrast, the neuronal dynamin1 appears in a burst at the site of dsRed-clathrin puncta immediately prior to internalization (Fig. 4). It has previously been suggested that dynamin1 and dynamin2 act as a 'pinchase' to sever formed clathrin-coated pits from the plasma membrane (Takei et al., 1995). However, it is possible that dynamin2 has alternate or additional functions before fission of the endocytic pit. The discrepancy observed between the behavior of dynamin1-EGFP and dynamin2-EGFP demonstrates the need for an evaluation of the functional differences between these molecules.

The finding that the amount of dynamin2 associated with clathrin puncta is linearly proportional to the amount of clathrin implies that there might be a direct coupling between these two proteins in endocytic pits. It is possible that the basis for the temporal, spatial and apparently stoichiometric relationship between clathrin and dynamin2 could follow from the recently proposed role for dynamin in actin organization (McNiven et al., 2000; Ochoa et al., 2000; Schmid and Sorkin, 2002). Although a role for dynamin in the remodeling of the actin cytosekeleton during cell migration has been observed (McNiven et al., 2000), it is not apparent whether this is based upon an affect on leading lamella extension, guidance of transport vesicles through the cortical actin network and/or actin based vesicle transport.

In addition to documenting the internalization of clathrin/dynamin2 spots (Figs 1, 4), these results characterize for the first time linear lateral motility of plasma membrane associated clathrin puncta (Fig. 1). Although some spots move laterally in the plane of the membrane and some are internalized, a large majority of spots are stationary over the time periods that were imaged (~60 seconds). Until a simultaneous analysis of receptor-ligand interactions and spot disappearance is performed, it will be unclear to what extent preformed clathrin spots may wait for activated receptors to cluster within them, or whether clathrin spots preferentially form at the sites of clustered activated receptors and/or move laterally to these same sites. Additionally, although the source of the motive force responsible for the lateral motility of dsRed-clathrin spots is currently unknown, the average rate measured (0.84 ± 0.10 μm second^{-1}) is comparable to values previously measured for microtubule motors (Apodaca, 2001) and myosin-V-based transport (Tabb et al., 1998).

Although some of the data obtained in the present studies provide a clear parallel with previous analyses of clathrin dynamics in living cells (Fig. 1) (Gaidarov et al., 1999), the finding that the distributions of numerous markers for clathrin-mediated endocytosis (clathrin, dynamin2 and transferrin) are polarized away from the lagging edge in migrating cells (Figs 6-8) represents a departure from models that suggest that cell migration requires increased endocytosis near the trailing edge and increased exocytosis near the leading edge (Bretscher, 1996; Palecek et al., 1996; Sheetz et al., 1999). What, then, is the role of endocytosis in cell migration? Is it to move and arrange adhesion molecules or is it to reinternalize membrane and proteins functional in membrane targeting and fusion (SNAREs etc.) following leading-edge exocytosis? It is possible that the coupling of exocytosis and endocytosis at the leading edge functions to adjust membrane tension to facilitate the generation of motile force by actin polymerization (de Curtis, 2001; Pollard et al., 2000; Watanabe and Mitchison, 2002). Alternatively, endocytosis at the leading edge might be important for the internalization of chemokine, cytokine and growth factor receptors. These questions await an integrated depiction of all of the constituent pathways potentially involved in cell migration (signaling, exocytosis, endocytosis and cytoskeletal organization).

Note added in proof

After this manuscript was submitted, a study was published [Merrifield et al. (2002). *Nat. Cell Biol.* **4**, 691-698] analyzing clathrin, dynamin1 and actin during endocytosis in 3T3 cells. Similarly to our results, they observed dyanamin1 associated with clathrin puncta just prior to endocytosis.

References

Altschuler, Y., Barbas, S. M., Terlecky, L. J., Tang, K., Hardy, S., Mostov, K. E. and Schmid, S. L. (1998). Redundant and distinct functions for dynamin-1 and dynamin-2 isoforms. *J. Cell Biol.* **143**, 1871-1881.

Apodaca, G. (2001). Endocytic traffic in polarized epithelial cells: role of the actin and microtubule cytoskeleton. *Traffic* **2**, 149-159.

Axelrod, D. (1981). Cell-substrate contacts illuminated by total internal reflection fluorescence. *J. Cell Biol.* **89**, 141-145.

Bajno, L., Peng, X. R., Schreiber, A. D., Moore, H. P., Trimble, W. S. and Grinstein, S. (2000). Focal exocytosis of VAMP3-containing vesicles at sites of phagosome formation. *J. Cell Biol.* **149**, 697-706.

Benmerah, A., Bayrou, M., Cerf-Bensussan, N. and Dautry-Varsat, A. (1999). Inhibition of clathrin-coated pit assembly by an Eps15 mutant. *J. Cell Sci.* **112**, 1303-1311.

Benmerah, A., Lamaze, C., Begue, B., Schmid, S. L., Dautry-Varsat, A. and Cerf-Bensussan, N. (1998). AP-2/Eps15 interaction is required for receptor-mediated endocytosis. *J. Cell Biol.* **140**, 1055-1062.

Bretscher, M. S. (1996). Moving membrane up to the front of migrating cells. *Cell* **85**, 465-467.

Cao, H., Garcia, F. and McNiven, M. A. (1998). Differential distribution of dynamin isoforms in mammalian cells. *Mol. Biol. Cell* **9**, 2595-2609.

Carter, R. E. and Sorkin, A. (1998). Endocytosis of functional epidermal growth factor receptor-green fluorescent protein chimera. *J. Biol. Chem.* **273**, 35000-35007.

Collins, B. M., McCoy, A. J., Kent, H. M., Evans, P. R. and Owen, D. J.

(2002). Molecular architecture and functional model of the endocytic AP2 complex. *Cell* **109**, 523-535.

Conrad, M. E., Umbreit, J. N. and Moore, E. G. (1999). Iron absorption and transport. *Am. J. Med. Sci.* **318**, 213-229.

de Curtis, I (2001). Cell migration: GAPs between membrane traffic and the cytoskeleton. *EMBO Rep.* **2**, 277-281.

Doxsey, S. J., Brodsky, F. M., Blank, G. S. and Helenius, A. (1987). Inhibition of endocytosis by anti-clathrin antibodies. *Cell* **50**, 453-463.

Engqvist-Goldstein, A. E., Warren, R. A., Kessels, M. M., Keen, J. H., Heuser, J. and Drubin, D. G. (2001). The actin-binding protein Hip1R associates with clathrin during early stages of endocytosis and promotes clathrin assembly in vitro. *J. Cell Biol.* **154**, 1209-1223.

Fenteany, G., Janmey, P. A. and Stossel, T. P. (2000). Signaling pathways and cell mechanics involved in wound closure by epithelial cell sheets. *Curr. Biol.* **10**, 831-838.

Fialka, I., Steinlein, P., Ahorn, H., Bock, G., Burbelo, P. D., Haberfellner, M., Lottspeich, F., Paiha, K., Pasquali, C. and Huber, L. A. (1999). Identification of syntenin as a protein of the apical early endocytic compartment in Madin-Darby canine kidney cells. *J. Biol. Chem.* **274**, 26233-26239.

Fuller, S. D. and Simons, K. (1986). Transferrin receptor polarity and recycling accuracy in 'tight' and 'leaky' strains of Madin-Darby canine kidney cells. *J. Cell Biol.* **103**, 1767-1779.

Gaidarov, I., Santini, F., Warren, R. A. and Keen, J. H. (1999). Spatial control of coated-pit dynamics in living cells. *Nat. Cell Biol.* **1**, 1-7.

Goldberg, M. B. (2001). Actin-based motility of intracellular microbial pathogens. *Microbiol. Mol. Biol. Rev.* **65**, 595-626.

Hopkins, C. R., Miller, K. and Beardmore, J. M. (1985). Receptor-mediated endocytosis of transferrin and epidermal growth factor receptors: a comparison of constitutive and ligand-induced uptake. *J. Cell Sci.* **3** (Suppl.), 173-186.

Jiang, W. and Hunter, T. (1998). Analysis of cell-cycle profiles in transfected cells using a membrane-targeted GFP. *Biotechniques* **24**, 349, 350, 352, 354.

Kamiguchi, H. and Lemmon, V. (2000). Recycling of the cell adhesion molecule L1 in axonal growth cones. *J. Neurosci.* **20**, 3676-3686.

Kamiguchi, H., Long, K. E., Pendergast, M., Schaefer, A. W., Rapoport, I., Kirchhausen, T. and Lemmon, V. (1998). The neural cell adhesion molecule L1 interacts with the AP-2 adaptor and is endocytosed via the clathrin-mediated pathway. *J. Neurosci.* **18**, 5311-5321.

Kirchhausen, T. (2002). Clathrin adaptors really adapt. *Cell* **109**, 413-416.

Lamaze, C. and Schmid, S. L. (1995). Recruitment of epidermal growth factor receptors into coated pits requires their activated tyrosine kinase. *J. Cell Biol.* **129**, 47-54.

Lampson, M. A., Schmoranzer, J., Zeigerer, A., Simon, S. M. and McGraw, T. E. (2001). Insulin-regulated release from the endosomal recycling compartment is regulated by budding of specialized vesicles. *Mol. Biol. Cell* **12**, 3489-3501.

McNiven, M. A., Kim, L., Krueger, E. W., Orth, J. D., Cao, H. and Wong, T. W. (2000). Regulated interactions between dynamin and the actin-binding protein cortactin modulate cell shape. *J. Cell Biol.* **151**, 187-198.

Merrifield, C. J., Moss, S. E., Ballestrem, C., Imhof, B. A., Giese, G., Wunderlich, I. and Almers, W. (1999). Endocytic vesicles move at the tips of actin tails in cultured mast cells. *Nat. Cell Biol.* **1**, 72-74.

Ochoa, G. C., Slepnev, V. I., Neff, L., Ringstad, N., Takei, K., Daniell, L.,

Kim, W., Cao, H., McNiven, M., Baron, R. et al. (2000). A functional link between dynamin and the actin cytoskeleton at podosomes. *J. Cell Biol.* **150**, 377-389.

Palecek, S. P., Schmidt, C. E., Lauffenburger, D. A. and Horwitz, A. F. (1996). Integrin dynamics on the tail region of migrating fibroblasts. *J. Cell Sci.* **109**, 941-952.

Pollard, T. D., Blanchoin, L. and Mullins, R. D. (2000). Molecular mechanisms controlling actin filament dynamics in nonmuscle cells. *Annu. Rev. Biophys. Biomol. Struct.* **29**, 545-576.

Raub, T. J. and Kuentzel, S. L. (1989). Kinetic and morphological evidence for endocytosis of mammalian cell integrin receptors by using an anti-fibronectin receptor beta subunit monoclonal antibody. *Exp. Cell Res.* **184**, 407-426.

Sabo, S. L., Ikin, A. F., Buxbaum, J. D. and Greengard, P. (2001). The Alzheimer amyloid precursor protein (APP) and FE65, an APP-binding protein, regulate cell movement. *J. Cell Biol.* **153**, 1403-1414.

Santini, F., Gaidarov, I. and Keen, J. H. (2002). G protein-coupled receptor/arrestin3 modulation of the endocytic machinery. *J. Cell Biol.* **156**, 665-676.

Schmid, S. L. (1997). Clathrin-coated vesicle formation and protein sorting: an integrated process. *Annu. Rev. Biochem.* **66**, 511-548.

Schmid, S. L. and Sorkin, A. D. (2002). Days and knights discussing membrane dynamics in endocytosis: meeting report from the Euresco/EMBL Membrane Dynamics in Endocytosis, 6–11 October in Tomar, Portugal. *Traffic* **3**, 77-85.

Schmoranzer, J., Goulian, M., Axelrod, D. and Simon, S. M. (2000). Imaging constitutive exocytosis with total internal reflection fluorescence microscopy. *J. Cell Biol.* **149**, 23-32.

Sheetz, M. P., Felsenfeld, D., Galbraith, C. G. and Choquet, D. (1999). Cell migration as a five-step cycle. *Biochem. Soc. Symp.* **65**, 233-243.

Sieczkarski, S. B. and Whittaker, G. R. (2002). Dissecting virus entry via endocytosis. *J. Gen. Virol.* **83**, 1535-1545.

Sun, T. X., van Hoek, A., Huang, Y., Bouley, R., McLaughlin, M. and Brown, D. (2002). Aquaporin-2 localization in clathrin-coated pits: inhibition of endocytosis by dominant-negative dynamin. *Am. J. Physiol. Renal Physiol.* **282**, F998-F1011.

Tabb, J. S., Molyneaux, B. J., Cohen, D. L., Kuznetsov, S. A. and Langford, G. M. (1998). Transport of ER vesicles on actin filaments in neurons by myosin V. *J. Cell Sci.* **111**, 3221-3234.

Takei, K. and Haucke, V. (2001). Clathrin-mediated endocytosis: membrane factors pull the trigger. *Trends Cell Biol.* **11**, 385-391.

Takei, K., McPherson, P. S., Schmid, S. L. and de Camilli, P. (1995). Tubular membrane invaginations coated by dynamin rings are induced by GTP-gamma S in nerve terminals. *Nature* **374**, 186-190.

ter Haar, E., Musacchio, A., Harrison, S. C. and Kirchhausen, T. (1998). Atomic structure of clathrin: a beta propeller terminal domain joins an alpha zigzag linker. *Cell* **95**, 563-573.

Tsuboi, T., Terakawa, S., Scalettar, B. A., Fantus, C., Roder, J. and Jeromin, A. (2002). Sweeping model of dynamin activity. Visualization of coupling between exocytosis and endocytosis under an evanescent wave microscope with green fluorescent proteins. *J. Biol. Chem.* **277**, 15957-15961.

Watanabe, N. and Mitchison, T. J. (2002). Single-molecule speckle analysis of actin filament turnover in lamellipodia. *Science* **295**, 1083-1086.